PRAMANA
— journal of
physics

Vol. 63, No. 4
October 2004
pp. 645–662

Physics of interferometric gravitational wave detectors

BIPLAB BHAWAL
LIGO Laboratory, California Institute of Technology, Pasadena, CA 91125, USA
E-mail: bbhawal@ligo.caltech.edu

Abstract. The Caltech-MIT joint LIGO project is operating three long-baseline interferometers (one of 2 km and two of 4 km) in order to unambiguously measure the infinitesimal displacements of isolated test masses which convey the signature of gravitational waves from astrophysical sources. An interferometric gravitational wave detector like LIGO is a complex, non-linear, coupled, dynamic system. This article summarizes various interesting design characteristics of these detectors and techniques that were implemented in order to reach and maintain its operating condition. Specifically, the following topics are discussed: (i) length sensing and control, (ii) alignment sensing and control and (iii) thermal lensing which changes the performance and operating point of the interferometer as the input power to LIGO is increased.

Keywords. Interferometer; gravitational wave; Laser Interferometer Gravitational-wave Observatory.

PACS Nos 04.30.Nn; 95.55.Ym; 07.05.Tp; 07.60.Ly

1. Introduction

The joint Caltech-MIT LIGO (Laser Interferometer Gravitational-wave Observatory) project [1] started the first science run of its three long-baseline interferometers (two at Hanford, Washington of baselines 4 km and 2 km and one at Livingston, Louisiana of baseline 4 km) in August 2002 for a duration of 17 days. The second and third science runs, each of continuous two months' operation, were carried out in February–April 2003 and November 2003 through January 2004 respectively. Since the beginning of 2002 when all three LIGO interferometers were brought to the operating condition called the 'locked' state, steady progress has been made to improve the noise level [2].

The aim of the designed LIGO is to achieve the required sensitivity in the audio frequency range up to a few kHz. Figure 1 shows expected contribution from various noise sources in the designed LIGO. The main known target sources of gravitational waves for LIGO are: (i) binary coalescing neutron star systems, (ii) rotating non-axisymmetric neutron stars, (iii) unmodeled sources like gamma ray bursts, supernova explosion etc., (iv) stochastic gravitational wave backgrounds of cosmological (primordial) and astrophysical origins. The most promising among

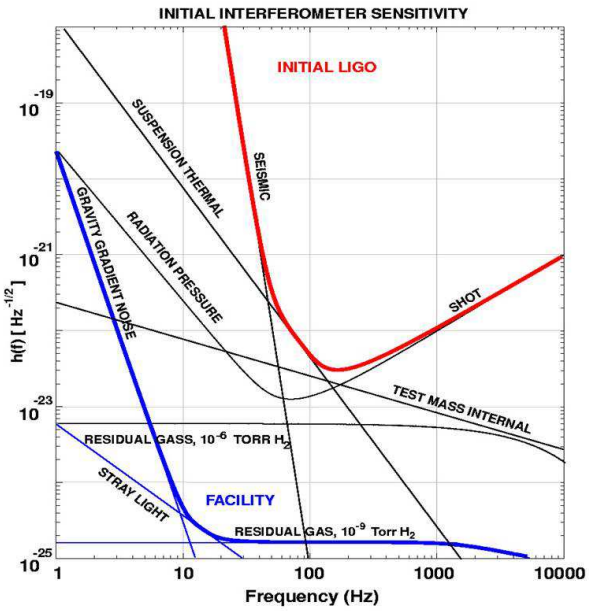

Figure 1. Noise curve for the designed LIGO. The main limiting noise sources are seismic, suspension and test-mass internal thermal and photon shot noise.

these known sources seems to be binary neutron star systems which contribute most of their signal-to-noise ratio in roughly 150–250 Hz range. So, the LIGO interferometers were designed to have its highest achievable sensitivity of about 10^{-18} m/$\sqrt{\text{Hz}}$ at around 200 Hz which translates into having the ability to measure the difference in length between the position of two test-masses (averaged out over the fluctuations of their atoms) to a precision of 1000th of nuclear diameter.

This is a challenging task and a lot of effort and innovation have been made to overcome this. Currently, LIGO is quite close to achieving the target sensitivity in the first generation of its detectors [2]. This article aims to discuss some interesting physics behind the design and operation of these interferometers and some key features and techniques employed to achieve successful operation of these complicated detectors. Because of the limited scope of this article, many topics will not be covered in detail here. A good account of the basic details and various physics issues may be obtained from Saulson's book [3].

In §2 the configuration of the LIGO detector and speciality of its features are discussed. Section 3 discusses the technique of Pound–Drever–Hall for extracting signal from a 2-mirror Fabry–Perot cavity for any phase offset inside it. Thereafter, the extension of this technique to the multi-cavity configuration of LIGO is introduced in §4. This section also discusses the problem of lock acquisition, i.e., reaching the operating state starting from the initial 'no light' condition. The length change due to low frequency tidal effect even when the interferometer is locked is also covered in § 4. The alignment of mirrors or beams in the interferometer is crucial for achieving the target sensitivity. This topic is covered in § 5. Section 6

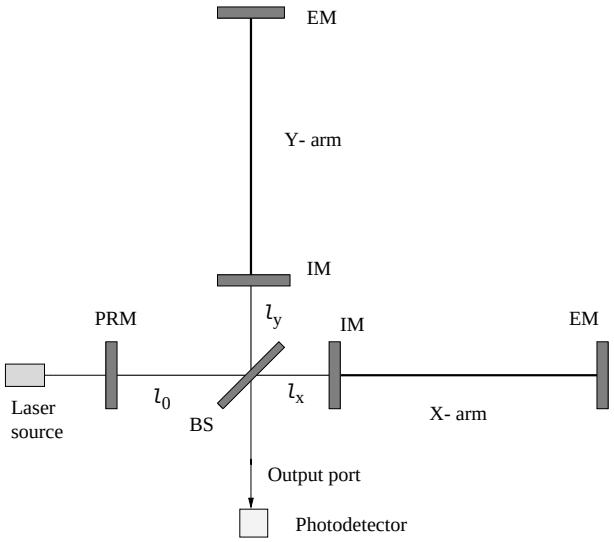

Figure 2. Configuration of power-recycled interferometer. BS, beam-splitter; EM, end mirror; IM, input mirror, PRM, power recycling mirror. Recycling cavity lengths, l_0, l_x, l_y are of the order of a few meters whereas arms are of 2 or 4 km length.

discusses the effect of thermal lensing that is encountered in LIGO as the input power is increased. Finally §6 summarizes some concluding remarks.

2. Configuration

The schematic in figure 2 shows the principal design features of the LIGO interferometers: (i) Fabry–Perot (FP) cavities are used in arms to increase the storage time of light, (ii) the lengths are adjusted so that the output port remains on the dark fringe for laser frequency in order to maximize the signal-to-noise ratio, (iii) in order to reduce photon shot noise, a high power laser is used and, under dark-fringe operation, the constructively interfered component of light that travels toward the laser source is recycled back to the interferometer by placing a suitable mirror in front of the source, thus enhancing laser power, (iv) all six mirrors are suspended like pendulums to filter out seismic noise above the resonant frequency of pendulum (at around 1 Hz) letting the mirror to move as free masses in the target bandwidth of detection (i.e. a few tens of Hz to several kHz).

The optical configurations of these detectors, with dynamics of mirrors involved, thus represent coupled, non-linear, multi-length systems with complicated dynamical responses. As shown in figure 3, the LIGO interferometer is a combination of two 3-mirror coupled cavities which themselves are coupled together through the beam-splitter. To explain its operation, it is essential to introduce some characteristics of the basic building block of its configuration: 2-mirror Fabry–Perot (FP) cavity.

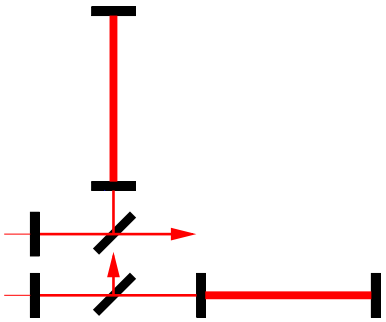

Figure 3. LIGO, as skeched in figure 2 could be thought of as a combination of two 3-mirror coupled cavities.

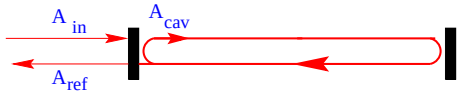

Figure 4. 2-mirror Fabry–Perot cavity.

2-Mirror Fabry–Perot cavity

Figure 4 shows a 2-mirror Fabry–Perot (FP) cavity. Under a resonant condition for the input light, the light newly introduced into the cavity interferes constructively with light from previous round-trips and thus the cavity enhances the power of the light inside the cavity. The amplitude of the internal light can be calculated to be the following Airy function, in which the phase offset, $\phi = 4\pi x/\lambda$ where $\lambda = 1.064 \times 10^{-6}$ m is the laser wavelength and x is a microscopic (i.e. $x/\lambda \ll 1$) length offset from the resonant length (i.e., $x = n\lambda - L$; where L is the actual length of the cavity):

$$A_{\rm cav} = A_{\rm in} \frac{t_i}{1 - r_i r_e {\rm e}^{i\phi}}, \tag{1}$$

$$\simeq A_{\rm in} \sqrt{\tilde{F}} \left(1 + i2\pi \frac{x}{\lambda/\tilde{F}}\right), \tag{2}$$

$$\tilde{F} = \left(\frac{t_i}{1 - r_i r_e}\right)^2 \simeq \frac{4}{t_i^2}. \tag{3}$$

The finesse $\tilde{F}$ determines how much gain the input power may get inside the cavity and the inverse of $\tilde{F}$ can be a measure of the width of the resonance curve. Basically, a higher value of $\tilde{F}$ means the cavity is more sensitive toward changes in longitudinal length. For LIGO arm cavity $\tilde{F}$ is about 133. The important point to note here is that the internal light amplitude gains an imaginary part in the presence of phase offset in cavity. So, the reflected light amplitude can be written as

$$A_{\rm ref} = r_i - t_i r_e {\rm e}^{i\phi} A_{\rm cav}. \tag{4}$$

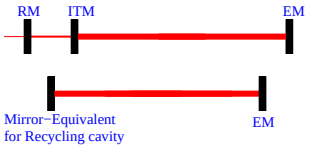

Figure 5. 3-Mirror coupled cavity and its equivalent 2-mirror cavity.

It may be noted that the addition of a recycling mirror enhances the finesse of the whole LIGO interferometer to a large extent – to a value of about 10000 – much larger than the finesse of individual arm cavity. As already noted, the full LIGO interferometer is a combination of two 3-mirror coupled cavities. Each of these 3-mirror systems can be treated as an equivalent 2-mirror cavity whose front mirror reflectivity is equal to the effective reflectivity of the recycling cavity constituted by the recycling mirror and input mirror as shown in figure 5. The effective reflectivity of this front mirror depends on the internal phase-offset of the recycling cavity and can be shown to reach a very high value near the combined resonance condition for the whole 3-mirror system (for mathematical details, see §§4 and 5 of ref. [4].)

In the next two sections we recall these facts about 2-mirror and 3-mirror systems to discuss the longitudinal length control issues of the full LIGO interferometer.

3. Length control of a Fabry–Perot cavity

Let us first discuss how to control the microscopic length of a 2-mirror Fabry–Perot cavity. From eq. (2) we can see that due to the presence of small phase offset from the resonance condition of the cavity, the internal light amplitude has got a small imaginary part. How to detect that part? One of the observables is power which can be calculated as

$$P_{\rm cav} = A_{\rm in}^2 \tilde{F} \times \left[1 - 4\pi^2 \left(\frac{x}{\lambda/\tilde{F}}\right)^2\right]. \tag{5}$$

The quantity $\lambda/\tilde{F}$ is of the order of 10^{-8} m. So, for the LIGO kind of length control and sensitivity, the effect on the internal power would be very small especially for the effect of squaring the very small length offset, x.

So, a technique that produces what is called Pound–Drever–Hall signal [5] is employed. As explained below, this signal is linear in phase offset x, very near the resonance. To introduce this technique and discuss the application of this in FP cavity and LIGO as such, let us introduce the concept of phase-modulation first.

The phase-modulated light is written as

$$\exp(i\omega_c t) \times \exp(i\epsilon_m \sin \omega_m t). \tag{6}$$

After expanding in terms of first-order Bessel functions, J_n, the above expression becomes

$$\exp(i\omega_c t) \times [J_0(\epsilon_m) + J_1(\epsilon_m)\mathrm{e}^{i\omega_m t} + J_{-1}(\epsilon_m)\mathrm{e}^{-i\omega_m t} + \cdots] \tag{7}$$

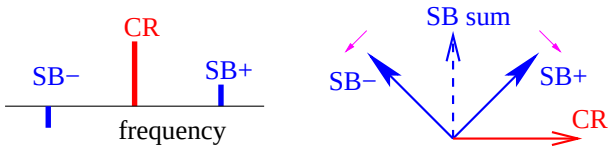

Figure 6. Left: Carrier and upper and lower sidebands. Right: Phasor diagram.

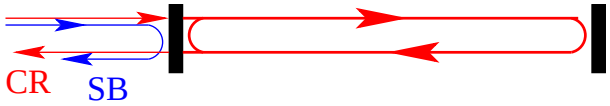

Figure 7. Carrier is resonant in cavity but sidebands are not.

which can be approximated as

$$\simeq \exp(i\omega_c t) \times \left[1 + \frac{\epsilon_m}{2} e^{i\omega_m t} - \frac{\epsilon_m}{2} e^{-i\omega_m t} + \cdots\right]. \tag{8}$$

We can see that, after phase modulation on the original frequency, which we will call the carrier frequency hereafter, mainly two more frequencies get created, $\omega_c \pm \omega_m$. These are called 'lower' and 'upper sidebands', SB^- and SB^+, as shown in figure 6.

From either eq. (6) or eq. (8) we can also write the following approximate equation:

$$\simeq \exp(i\omega_c t) \times [1 + i\epsilon_m \sin \omega_m t]. \tag{9}$$

Referring to the phasor diagram in figure 6, we can say that the sidebands are rotating with respect to the carrier in opposite directions but their sum is always orthogonal to the carrier.

Let us now enter this phase-modulated light in a Fabry–Perot cavity as shown in figure 7. The cavity is made resonant with respect to the carrier and so the sidebands get reflected from the front mirror but the carrier gets built up inside the cavity. If there is any phase change inside the cavity, the carrier light experiences this offset and the leaked out part of the carrier at the reflected port brings that information with it. The sidebands, by not being inside the cavity, do not experience the phase shift and so can be used as reference or local oscillator. One can get signal for this phase shift by beating the carrier with sidebands.

So, the power of the reflected light becomes

$$|\overline{\mathrm{CR}} + \overline{\mathrm{SB}}^+ + \overline{\mathrm{SB}}^-|^2. \tag{10}$$

The radio frequency amplitude-modulated part of this light is

$$2 \times \mathrm{Real}(\overline{\mathrm{CR}}^* \times [\overline{\mathrm{SB}}^+ + \overline{\mathrm{SB}}^-]) = 2 \times \mathrm{Real}(\overline{\mathrm{CR}}^* \times i\epsilon_m \sin \omega_m t). \tag{11}$$

In the above equation the sum of the sideband amplitudes is replaced by the term from eq. (9). As we have seen in eq. (2), in the presence of phase-offset, the carrier

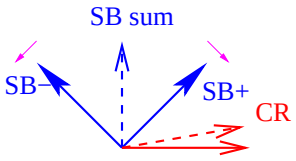

Figure 8. Phasor diagram: Carrier gained an imaginary part from phase-offset.

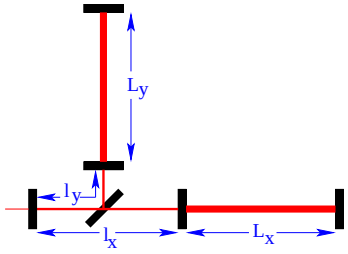

Figure 9. LIGO cavity lengths.

light gains an imaginary part which we represent below as Φ. So, we get a signal which is proportional to

$$\text{Real}((1 + i\Phi) \times i\epsilon_m \sin \omega_m t) = \epsilon_m \Phi \sin \omega_m t. \tag{12}$$

The phasor diagram of this situation is represented in figure 8. This is then demodulated (essentially multiplying with an oscillator of frequency, ω_m) to get signal proportional to

$$\epsilon_m \Phi \sin^2(\omega_m t) = \frac{1}{2}\Phi\epsilon_m(1 - \cos 2\omega_m t) \tag{13}$$

which is then passed through a low-pass filter to get the signal at a RF photodiode. The final signal is linear in $\Phi : \epsilon_m \Phi$.

One may note that by applying this technique the phase change in light is effectively transformed into the amplitude change of the light. In the next section we discuss how this is extended to extract length offset signals for a multi-cavity coupled system like LIGO.

4. Length control of LIGO and lock-acquisition

As shown in figure 9, LIGO has four length degrees of freedom for the four resonant lengths involved. A better way of representing these is a set of their linear combinations:

1. Common modes: $\ell^+ = (\ell_x + \ell_y)/2\,, \quad L^+ = (L_x + L_y)/2.$
2. Differential modes: $\ell^- = (\ell_x - \ell_y)/2\,, \quad L^- = (L_x - L_y)/2.$

The differential mode, L^-, represents the measure of opposite effects (of contraction and expansion) in two arms. The polarization of gravitational wave may effect such changes in the arms.

The common mode, L^+, represents the measure when both arms are contracting or expanding in the same way at the same point of time. One must note that, apart from actual length changes like this which may originate from seismic noise, this mode could also have contribution from changes in laser frequency. Any change in frequency, ω, of the laser affects both arms in the same way and so may manifest itself as common mode:

$$\frac{\Delta\omega}{\omega} = \frac{\Delta L}{L}. \tag{14}$$

Implementation of a feedback control system requires a detection scheme which can separably sense all longitudinal degrees of freedom. We discuss now how the signals are extracted from the interferometer to determine these four modes and are fed back to the mirrors and laser to make microscopic length adjustments and also to laser to correct the frequency or supress its noise. It may be noted that, due to inherent (and possibly unavoidable) asymmetries between two arms of the as-built LIGO, the full effect of common modes do not manifest itself as purely 'common' effect on the field evolution in the interferometer. Some part may show up as differential effect and vice versa. For example, any change in position of the recycling mirror changes both ℓ_x and ℓ_y in the same way and so is a common mode. If the interferometer is operating under the dark fringe condition, no carrier light should escape the output port (refer to figure 2) due to this motion in recycling cavity. However, if the reflectivities of the arms are different, the interference of the lights from arms at this port will not be fully destructive and so some carrier light should escape through this port. This is a manifestation of differential mode, even though actual length changes are common in nature.

The technique described in the last section is extended to control the full LIGO system [6]. The main operating criterion is that the carrier should be made resonant to all cavities in the full interferometer. To bring the system to this state and to control length offsets from this state, laser light is phase modulated before it enters the interferometer and the sidebands are made resonant only in the recycling cavity. These do not enter the arm cavities and so, just like in the case of FP cavity, do not experience any phase changes in arm cavities and can act as local oscillators.

The lengths of the recycling cavity in x- and y-directions are made a little different to allow some sideband light to leak to the *dark* port (this is known as 'Schnupp asymmetry'):

$$P_{\mathrm{SB}}(\mathrm{dark}) \propto [\omega(\ell_x - \ell_y)/c]^2. \tag{15}$$

The recycling cavity mirror transmittivities are such that the cavity is very close to being *symmetric*. A perfectly *symmetric* FP cavity can be defined as one whose front and end mirrors have same reflectivities but no losses. For such a cavity the input light completely transmits out through the cavity. The as-built recycling cavity mirrors of LIGO have losses and also there exists some difference in reflectivities of the recycling mirror and the input mirrors. However, we can say that it is very close to what a symmetric cavity is and so we expect that almost all of the sideband

light that falls on the recycling mirror to enter the interferometer should get transmitted through the dark port. Note that the sidebands cannot get transmitted into arms because, as already mentioned, the arms are held at anti-resonant condition for the sidebands. A measure of how efficiently sidebands leak out through the output port is known as sideband efficiency. This number may turn out to be much less than the perfect value of 100% depending on heating of mirrors by the laser light and the consequent effect of thermal lensing that we introduce and discuss in §6.

Whenever, for example, due to some differential length changes, some carrier light leaks into the dark port, it beats with the sideband lights already present there and gives the Pound–Drever–Hall signal for differential length changes.

Similarly for other modes and frequency noises, similar signals are collected from other ports, like the reflected port and internally from the beam-splitter. In an ideal situation with a proper choice of ports and signals, the correspondence between signals and degrees of freedom should be one-to-one or, in other words, their relationship can be expressed as a diagonal matrix. This matrix can be inverted and proper conversions can be made to find out how much force need to be applied through the actuators to each mirror to control the full interferometer. However, for various reasons including the one that the as-built interferometer is not really symmetric in two directions, the matrix may not turn out to be diagonal and this may cause a lot of difficulty in the control of the full system. The problem finally becomes one of finding the proper basis in which the matrix may become close to the diagonal.

One must note again that the Pound–Drever–Hall signals are linear when the interferometer is very close to its operating point and the deviations are just fractions of the laser wavelength of 1.064 μm (say, 1/1000th for differential mode. For common mode, the limit could be much more stringent, about $1/10^7$th).

So, one of the expected main problems in the first year of LIGO commissioning (year 2000) was to start from no light condition in the interferometer and bring it to the desired operating condition called the locked state when carrier is resonant throughout and sidebands are resonant only in recycling cavity. As already explained, because of the coupled nature of all the cavities and the low frequency seismic noise that constantly drives the mirrors, this transition needs to pass through lot of states when none or only one or two of the cavities are resonant at a time. Also we can recall from our discussion of 3-mirror coupled system in §2 that closer to the final operating condition, the effective finesse of the whole system for the carrier frequency becomes quite high and various non-linear effects also come into account.

Due to these reasons the problem of achieving the desired locked state starting from the first entry of light through the recycling mirror is not a trivial problem. The aim is to acquire lock by initially stabilizing the relative optical positions to establish the resonance conditions and bring them within the linear regions of the error signals and then to maintain the interferometer at the operating point by using linear time-invariant feedback from a phase-modulation–demodulation system that provides linear error signals for small deviations from the operating point.

However, the probability of all the four degrees of freedom being simultaneously within ≈ 1 nm or even shorter (for some modes) linear region of the resonance points

is extremely small, and thus a sequential locking approach is adopted, whereby all degrees of freedom are captured in sequence. Such an approach needs a good step-by-step algorithm that takes into account evolution of fields due to mirror motion and changing resonant conditions of various cavities that are coupled to each other. This is where the time-domain simulation of the interferometer played a very important role.

In order to have an insight into the complex field evolution in a complicated system like LIGO with so many degrees of freedom, the study of the system by computer simulation is essential. With that objective, a simulation package with various modeling tools has been developed at Caltech. This simulation program called LIGO end-to-end (E2E) model [7] allows us to perform computer experiments on LIGO or its advanced design-variants or on some subsystems of it. The E2E package simulates the time-evolution of fields, optics, mechanical structures and electronic and control systems. It can be viewed as a software toolbox, like MATLAB [8], and complex systems can be simulated by combining building blocks.

In order to help LIGO commissioners in the lock acquisition effort, a model of the interferometer was built up using the E2E package in the later half of 2000 [9]. Its purpose was to design and develop the Hanford 2 km interferometer locking servo and simulate the major characteristics of length degrees of freedom under 20 Hz. Using this model an algorithm was developed that could sequentially bring into lock the various degrees of freedom by use of measurable optical signals to estimate the time-evolving sensing matrix and application of feedback forces to reduce the mirrors' relative velocities.

This model took the following into consideration: (i) Only longitudinal degrees of motion were considered everywhere (field evolution with scalar field approximation), (ii) effects of saturation of actuators, (iii) simplified seismic motion and correlation, (iv) analog length sensing and control (LSC) system; the alignment sensing and control system was not modeled, (v) frequency noise, shot noise and sensor, actuator and electronic noise were not included.

Figure 10 shows the step-by-step locking procedure followed for the full interferometer [10]. The corresponding lock-acquisition code was developed in E2E. Essentially this code calculates signals at different states and invert those to the force necessary to move the mirrors in appropriate direction depending on the current state of the interferometer and in that way proceed toward the final operating condition. This code was directly ported to the real interferometer control system. When the actual interferometer acquired locked state, any typical field-evolution curve, as shown in figure 11, followed essentially the same pattern in going from state to state as observed in time-domain simulation runs.

This same algorithm is used to lock all LIGO interferometers. Nowadays, under a normal condition, any interferometer takes only a few minutes to get into the locked state.

We may note that even under a locked state, the suspension points of the LIGO mirrors may get slowly displaced due to the residual, very low-frequency components of the seismic noise originating mainly from tidal effects. As the difference between two suspension points gets shorter or longer, it becomes harder for the control system to maintain the length between mirrors in resonant condition. The LIGO arms experience Earth- and Sun-induced daily strains of the order 3×10^{-8}.

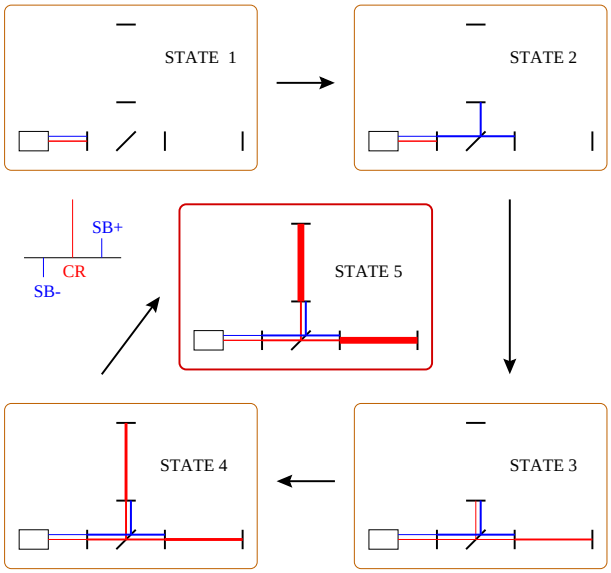

Figure 10. States of lock acquisition. State 1: Light just enters through the recycling mirror; nothing is controlled. State 2: Sidebands (SB) resonate in the recycling cavity; the same cavity is held on a carrier (CR) anti-resonance. State 3: One of the end mirrors is controlled and carrier resonates in that controlled arm. State 4: The other ETM is controlled and carrier resonates in both arms and the recycling cavity. State 5: Power in the full interferometer is stabilized at its operating level.

With kilometer scale arms, these strains exceed the limited range of the quiet, high bandwidth control servos keeping the optics positioned within a 1/4 wavelength of the resonating light of 1 μm wavelength. While these control systems have a range of a few tens of micrometers, the daily strains will typically approach 120 μm.

Monitoring of tidal effects is thus absolutely necessary for continuous operation of the interferometer. In LIGO the common mode tidal effects are controlled by adjusting the carrier wavelength which, as already described, affects both arms. The differential mode is dealt with separately for each arm and this is effected by physically moving the structure of the optical mounting platform.

In the next section, we discuss the effect of misalignments of the mirrors which may originate from seismic noise or from any defect in suspension system. An initial 'gross' reduction of the level of misalignments in mirrors below a certain level is essential for achieving or maintaining lock. However, under a locked state, a very good level of alignment of optics is necessary to achieve the desired sensitivity.

5. Alignment control

While maintaining the longitudinal separations between the test mass mirrors is crucial to optimize the intensity of the light circulating in the interferometer,

maintaining the maximum phase sensitivity crucially depends on the alignment of the optical components with respect to the incoming beam [11].

Just like in the section on length control, let us discuss this first in terms of a 2-mirror FP cavity. A stable FP cavity has its own set of eigenmodes whose basis is defined by mirror radii of curvature and length. The eigenmodes may be expressed in terms of Hermite–Gaussian functions [12] which are combinations of Hermite polynomials and Gaussian functions. A beam which matches the eigenmode of the cavity can be expressed in terms of two quantities, the waist size, W_0 and the location of the waist, Z, as shown in figure 13. These quantities can be directly calculated from the cavity parameters: length and mirror radii of curvature [12]. The fundamental mode of this basis is a purely Gaussian function which means that a transverse cross-section of a beam which is perfectly resonant in a cavity shows a purely Gaussian distribution of power.

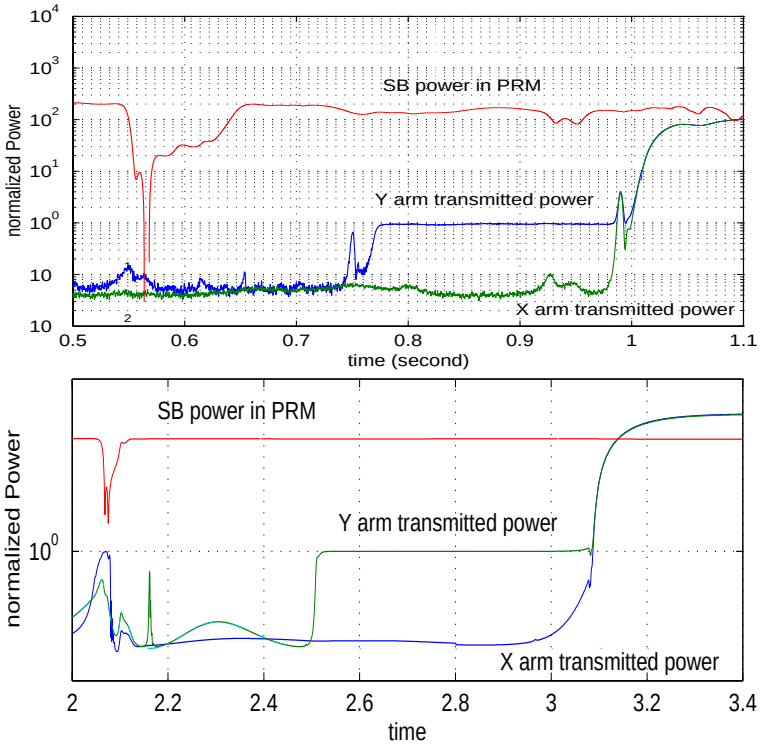

Figure 11. The lock-acquisition of Hanford 2 km interferometer. The top plots are from the actual lock acquisition process in the physical interferometer and the bottom plots correspond to those from E2E's simulation set-up. Both plots show changes in power as the interferometer goes from one state to the other for finally acquiring the full locked state. The sideband (SB) power in PRM (power recycling cavity) is normalized to the input sideband power multiplied by the RM transmittivity, whereas the other two curves in both plots are normalized to the one arm transmitted power in the absence of RM.

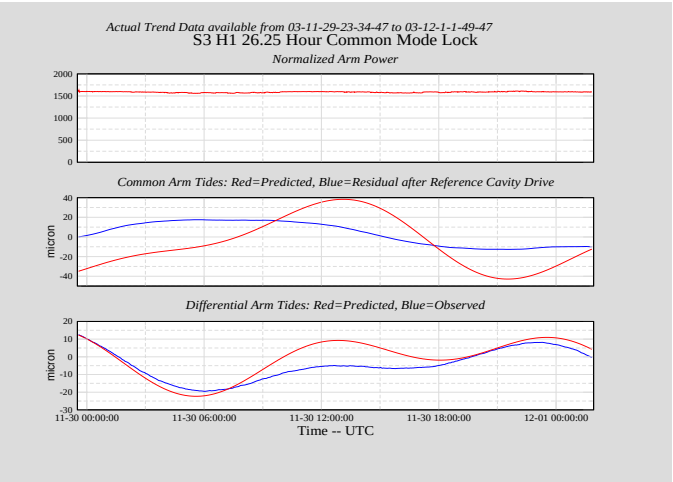

Figure 12. Tidal effect on arms: Shown in a 24 h locked stretch of Hanford 4 km interferometer. Top: Normalized arm power showing the locked strech. Middle: red – prediction of common mode tidal stretching. Blue – observed displacement measured from fine actuators at the end stations; measurement done after compensating the laser frequency. Bottom: red – predicted differential mode. Blue – observed differential correction required to maintain resonance.

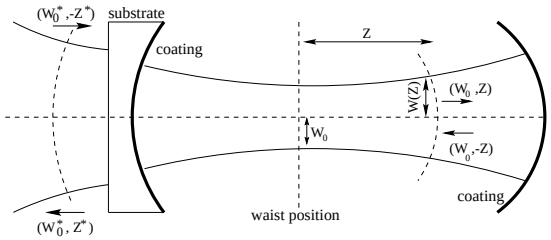

Figure 13. Fundamental eigenmode of a Fabry–Perot cavity.

Let us represent the unperturbed beam of wave number K and waist size, W_0, at the waist location ($Z = 0$) as AU_0, where A is the amplitude and U_0 is the fundamental TEM00 mode of the beam. Then various kinds of perturbations as shown in figure 14 generate higher order modes represented by U_i, $i = 1, 2, \ldots$ (only the first 2 ($i = 1, 2$) higher order modes are shown in these equations):

1. Rotation (ρ): $A[U_0 + i\rho\frac{KW_0}{\sqrt{2\pi}}U_1]$,
2. Lateral displacement (d): $A[U_0 + \sqrt{\frac{2}{\pi}}\frac{d}{W_0}U_1]$,
3. Waist-position mismatch (b): $A[U_0 + i\frac{b}{2KW_0^2}U_0 + U_2]$,
4. Waist-size mismatch (difference between new and old waist size (s): $A[U_0 + \frac{s}{2W_0}U_2]$.

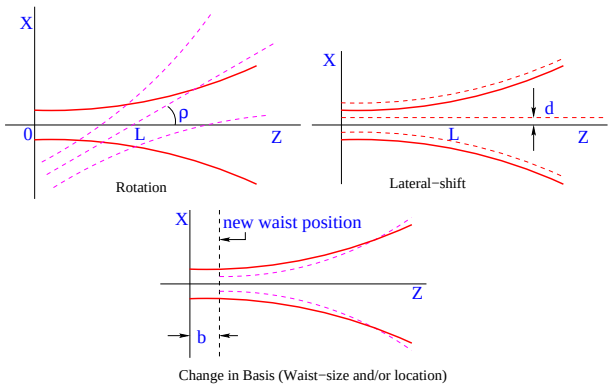

Figure 14. Perturbations on beam.

These perturbations can be effected in a LIGO system by rotation or transversal shift of the mirrors. The perturbations 3 and 4 can be caused by sending a wrongly focussed beam into the interferometer or may originate from thermal lensing effect (to be discussed in the next section). These types of misalignments of the components of the interferometer with respect to the incident laser light cause light in the fundamental mode of the cavity to couple into higher order modes. This reduces the amount of power circulating in the arm cavities due to reduced coupling of light into them, resulting in reduced phase sensitivity. Also the higher order modes leaking out the signal extraction port of the interferometer result in increased photocurrent and shot noise.

For the sensing and control of misalignments or the beam wavefront, a variant of the Pound–Drever–Hall locking technique is employed. Each mirror has two degrees of rotation: pitch (around the horizontal x-axis) and yaw (around the vertical y-axis). So, digital control of 12 mirror angles (pitch and yaw modes for each of 6 mirrors) and the input beam direction has been implemented. The target of this alignment sensing and control system is to suppress angular fluctuations of all mirrors below 10^{-8} rad (rms value).

Figure 15 explains the basic principle of wave-front sensing (WFS) for a 2-mirror FP cavity. For the full LIGO system, in order to control all six mirrors and the direction of the input beam, four WFS systems are utilized to collect misalignment signals for various degrees of freedom. Just like in length control system, in this case too, the signals are mixed up and proper basis needs to be carefully chosen in order to make one-to-one correspondence between a signal and a particular mode. The matrix representing this relationship is then inverted and actuators in mirrors and/or in the telescope sending the input light to the interferometer are activated to control the whole system. Figure 16 shows how the interferometer performance improves after activating the WFS system.

6. Thermal lensing

The target sensitivity of LIGO requires the use of very high light power, 20 kW in arms, to reduce the photon shot noise. Absorption of a small fraction of this power

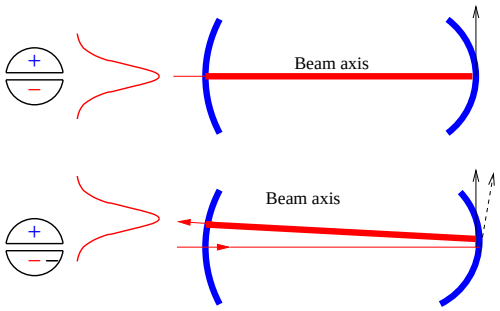

Figure 15. Basic principle of wavefront sensing: In an unperturbed state (upper figure), the beam in the cavity is in the same basis as of the input beam and its axis is the same as the cavity axis. Thus the split photodetector that is aligned with the cavity axis measures same power in both parts. The signal which is a difference of these two parts is thus zero. When, for example, the end mirror rotates at microradian level, the internal light mode is different from the input light fundamental mode – the internal beam axis rotates with respect to the input beam and the reflected light beam center gets shifted. The split photodetector now measures power more in the upper plane than in lower plane and a non-zero signal with sign for the direction of rotation can be obtained. Note that LIGO actually uses quadrant photodetectors but employs the same principle to sense rotation around both vertical (yaw mode) and horizontal (pitch-mode) directions.

in the optical components can lead to serious degradation of the performance of the interferometer.

The temperature gradient inside the substrate leads to the gradient of refractive index and thus optical path length across transverse direction. This leads to changes in transmitted beam wavefront and is called thermal lensing [13].

In LIGO I, the main contribution of this effect comes from the input mirror. So, even if the input light is prepared to be the fundamental eigenmodes of the cavities, due to thermal lensing the light may still be mode-mismatched and so not perfectly resonant in the cavity. Analytical calculation and some careful FFT modeling show that there is a negligible effect of thermal lensing on the carrier in LIGO first generation interferometer because the carrier modes are mainly determined by arms which are large compared to the recycling cavity.

However, the situation is different for sidebands which are coupled into only the recycling cavity and does not enter the arms. The recycling cavity length (about 9 m) is much smaller than the radii of curvature (about 15 km) of the recycling mirror or the input mirrors constituting the cavity. Under such a situation, the cavity approaches a degenerate state which means it does not have any preferred eigenmode to select. This is a serious situation because most of the higher order modes that may get created due to any kind of perturbation may get resonant in such a cavity and, with much of the higher order modes, the cavity may become unstable.

Thermal lensing affects the mode-matching of the sidebands in a big way as it goes through the dielectric of the input mirrors, gets totally reflected from its

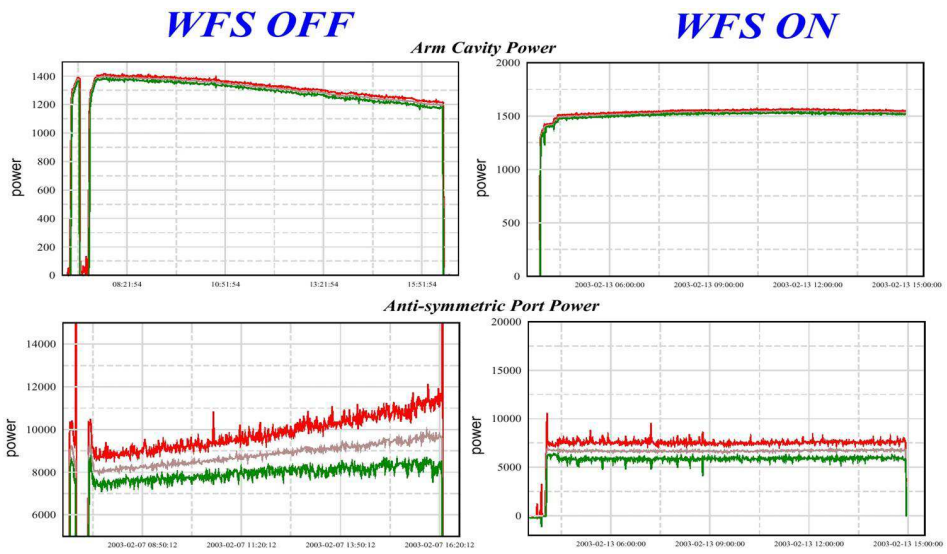

Figure 16. Wavefront sensor (WFS) and the control system improves the interferometer performance. The top figures show how the arm cavity power got stabilized when WFS is on. If WFS is not working, even though the interferometer is locked, the power starts decreasing due to the presence of misalignments as shown in the locked stretch of about 9 h in left-side figures. More power get leaked out of the dark port (bottom left) and contributes more to the shot noise level. Finally the whole system may go out of lock. The right-side figures show much more stabilized performance for a locked stretch of more than 11 h when WFS is on.

surface and gets into the recycling cavity again. The amount of heat absorbed in the input mirror has two components:

$$\text{Substrate heat absorption} = \text{Input power} \times \text{Recycling gain} \times \text{Substrate absorption coefficient}, \tag{16}$$

$$\text{Surface heat absorption} = \text{Input power} \times \text{Recycling gain} \times \text{Arm gain} \times \text{Surface absorption coefficient}. \tag{17}$$

In LIGO I, the input power entering the recycling mirror is about 6 W, the recycling gain is about 50 and the arm gain is about 133. So, the power in recycling cavity between the recycling mirror and beam-splitter is about 150 W, while the arm power is about 20 kW. Note that in eq. (17) only the surface absorption from the arm side of the input mirror(s) is considered because its effect is much more than the absorption from the recycling cavity side. Any difference in these absorption coefficients and reflectivities (which determine gains) between optics in two arms causes difference in the level of mode-matching in two sides of the interferometer and may lead to more difficulties in its operation.

Figure 17 shows the effect of thermal lensing on the carrier and the sidebands. The cross-section of the carrier intensity remains to be Gaussian or the fundamental mode. However, the sideband cross-section shows a combination of various

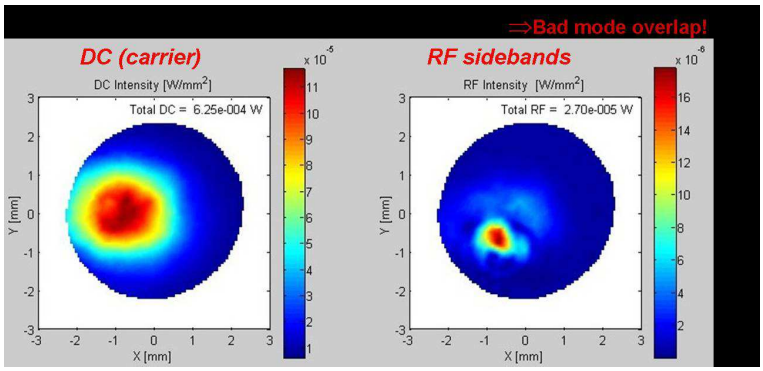

Figure 17. The effect of thermal lensing: Note how the sideband beam profile gets distorted and becomes non-Gaussian due to bad mode matching and consequent generation of higher order modes. Carrier beam profile does not get affected and remains Gaussian. Without thermal lensing their profiles should look similar.

unwanted higher order modes. This affects the sideband efficiency which could get reduced to a value of mere 6%. So, less (than designed $\approx$ 100%) sideband power gets into the dark port and also the overlap of sidebands with carrier for producing the signal (the scalar product) gets much reduced.

As a remedy for this situation, a program of thermal compensation of the mirrors in the Hanford 4 km detector started in the beginning of 2004. The aim of this program is to nullify the effect of thermal lensing by heating the input mirrors. For the first attempt, CO_2 laser is directly projected onto the mirrors to heat them up and the phase maps of light are monitored to determine the exact amount of heat needed to be deposited to nullify the thermal lensing in each input mirror. This attempt has progressed with satisfaction and the sideband efficiency could be increased to a good level. One can hope that this improvement will contribute a lot in the operation and performance of the detectors during the fourth science run scheduled in the last quarter of 2004.

7. Concluding remarks

In this article we covered the three most essential features of operation of the first generation of LIGO interferometers, namely, length control, alignment control and compensation of thermal lensing. A number of other essential features of LIGO such as seismic isolation system, suspension system and its local control, stabilization of amplitude and frequency of the beam before it enters the interferometer, etc. have not been discussed. Discussion of many other important features and techniques which have played crucial roles in reducing the noise level has also been avoided in the limited scope of this article.

The milestone of touching the LIGO designed sensitivity seems to be very close at the time of writing this article. The design of the advanced LIGO interferometer

and its subsequent operation and the ensuing struggle to take the sensitivity level up by another order of magnitude will bring new challenges to the LIGO team.

Acknowledgements

Thanks to all LIGO Laboratory colleagues at Caltech, MIT and the Observatory sites at Hanford and Livingston for various studies and measurements which have been used to illustrate various issues in this article. Special thanks are due to M Evans, A Lazzarini, H Radkins, R Savage and Hiro Yamamoto for their help and comments. The LIGO Observatories were constructed by the California Institute of Technology and Massachusetts Institute of Technology with funding from the National Science Foundation under cooperative agreement PHY 9210038. The LIGO Laboratory operates under cooperative agreement PHY-0107417. This article is assigned LIGO document number LIGO-P040005-00-E.

References

[1] B Barish and R Weiss, *Phys. Today* **52**, 44 (1999)
LIGO home page http://www.ligo.caltech.edu
[2] G González, *Pramana – J. Phys.* **63**, 663 (2004)
[3] P Saulson, *Fundamentals of interferometric gravitational wave detectors* (World Scientific, 1994)
[4] B Bhawal, *J. Opt. Soc. Am.* **A120**, 15 (1998)
[5] R W P Drever, J L Hall, F V Kowalski, J Hough, G M Ford, A J Munley and H Ward, *Appl. Phys.* **B31**, 97 (1983)
[6] P Fritschel, R Bork, G Gonzalez, N Mavalvala, D Ouimette, H Rong, D Sigg and M Zucker, *Appl. Opt.* **40**, 4988 (2001)
[7] B Bhawal, M Evans, M Rakhmanov, V Sannibale and H Yamamoto, *Proceedings of the XXXVIIIth Rencontres de Moriond Workshop on Gravitational Waves and Experimental Gravity*, Les Arcs, France, 22–29 March, 2003, edited by J Dumarchez and J Tran Thanh Van (The Gioi Publishers, Vietnam, 2004) pp. 131–138
[8] MATLAB, A technical computing software package developed by the Mathworks Inc. (http://www.mathworks.com)
[9] M Evans, Lock acquisition in resonant optical interferometers, Ph.D. Dissertation (Caltech, Pasadena, 2001)
[10] M Evans, N Mavalvala, P Fritschel, R Bork, B Bhawal, R Gustafson, W Kells, M Landry, D Sigg, R Weiss, S Whitcomb and H Yamamoto, *Opt. Lett.* **598**, 27 (2002)
[11] P Fritschel, N Mavalvala, D Shoemaker, D Sigg, M Zucker and G Gonzalez, *Appl. Opt.* **28**, 37 (1998)
[12] A E Siegman, *Lasers* (University Science Books, Sausalito, CA, 1986)
[13] P Hello and J Y Vinet, *J. Phys. (Paris)* **51**, 2243 (1990)
W Winkler, K Danzmann, A Rüdiger and R Schilling, *Phys. Rev.* **A44**, 7022 (1991)